Supplemental Material

Journal of Climate
Reduced Evapotranspiration Decreases Land Precipitation despite Enhanced Moisture Convergence: Insights from Perturbed Parameter Ensembles of Earth System Models
https://doi.org/10.1175/JCLI-D-25-0739.1

© Copyright 2026 American Meteorological Society (AMS)
For permission to reuse any portion of this work, please contact permissions@ametsoc.org. Any use of material in this work that is determined to be "fair use" under Section 107 of the U.S. Copyright Act (17 USC §107) or that satisfies the conditions specified in Section 108 of the U.S. Copyright Act (17 USC §108) does not require AMS's permission. Republication, systematic reproduction, posting in electronic form, such as on a website or in a searchable database, or other uses of this material, except as exempted by the above statement, requires written permission or a license from AMS. All AMS journals and monograph publications are registered with the Copyright Clearance Center (https://www.copyright.com). Additional details are provided in the AMS Copyright Policy statement, available on the AMS website (https://www.ametsoc.org/PUBSCopyrightPolicy).

Generated using the official AMS LaTeX template v6.1

Supplemental Material for "Reduced Evapotranspiration Decreases Land Precipitation Despite Enhanced Moisture Convergence: Insights from Perturbed Parameter Ensembles of Earth System Models"

Benjamin G. Buchovecky,[a] F. Hugo Lambert,[b] Claire M. Zarakas,[a] Marysa M. Laguë,[c] Charlie D. Koven,[d] Inez Y. Fung,[e] David B. Bonan,[a,f] Abigail L. S. Swann[a,g]

[a] *Department of Atmospheric and Climate Science, University of Washington, Seattle, Washington*

[b] *Department of Mathematics and Statistics, University of Exeter, Exeter, United Kingdom*

[c] *Department of Geography, University of British Columbia, Vancouver, Canada*

[d] *Climate and Ecosystem Sciences Division, Lawrence Berkeley National Laboratory, Berkeley, California*

[e] *Department of Earth and Planetary Science, University of California, Berkeley, California*

[f] *Cooperative Institute for Climate, Ocean, and Ecosystem Studies, University of Washington, Seattle, Washington*

[g] *Department of Biology, University of Washington, Seattle, Washington*

Corresponding author: B. G. Buchovecky, bbucho@uw.edu

Contents of this file

1. Supplemental Figures S1 to S9
2. Supplemental Tables S1 to S4

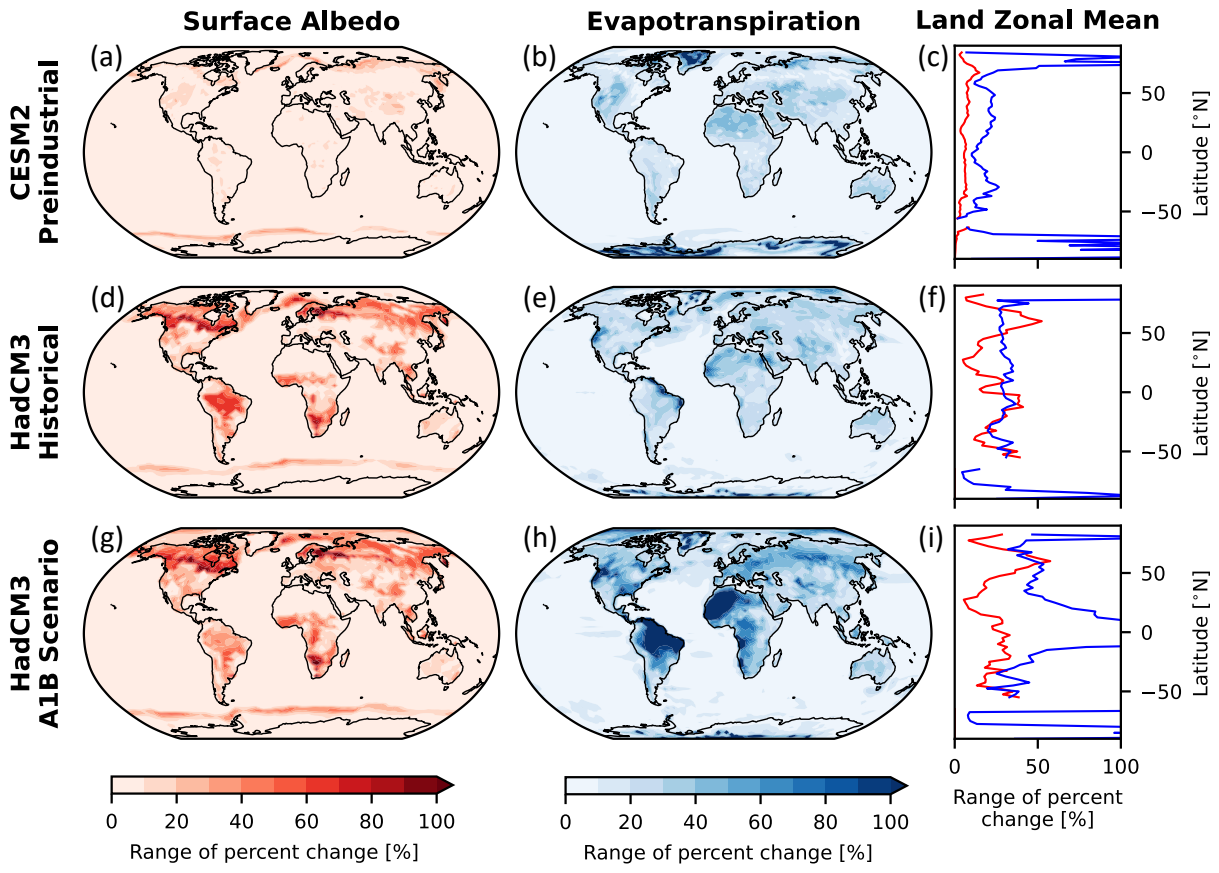

FIG. S1. Maps of the range of percent change in grid point surface albedo (left column) and evapotranspiration (center column) across each PPE (rows). The right column displays the zonal mean range of percent change in surface albedo (red line) and evapotranspiration (blue line).

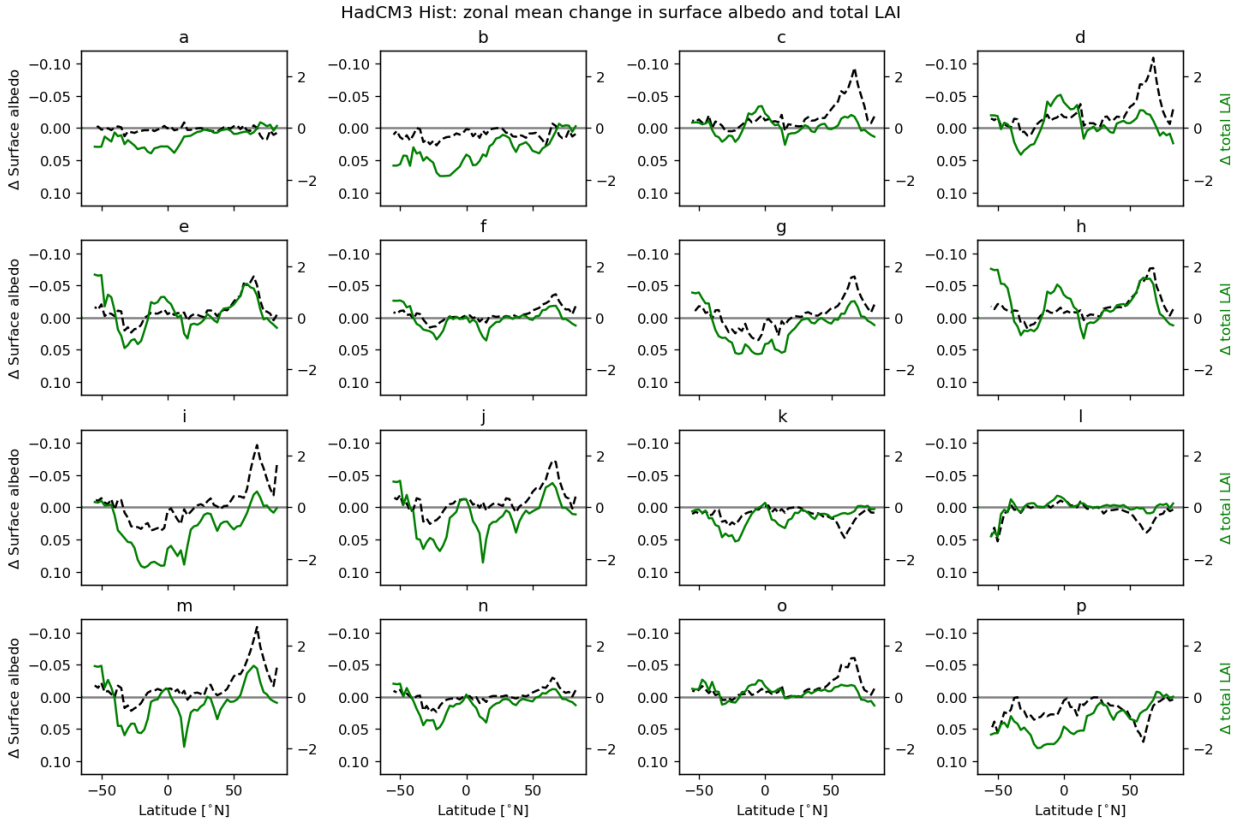

FIG. S2. The zonal mean changes in surface albedo (black dashed line) and total leaf area index (green line) across each ensemble member of the HadCM3C Hist PPE.

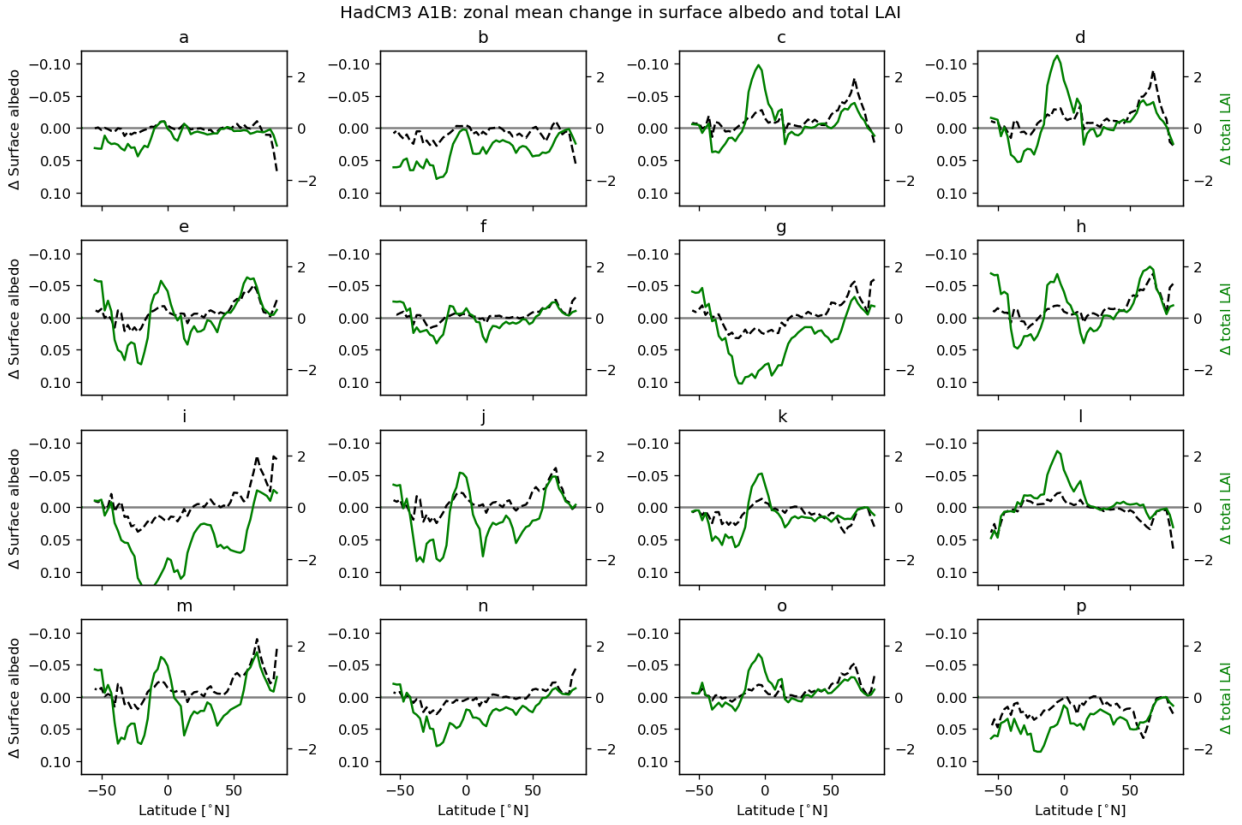

24 FIG. S3. The zonal mean changes in surface albedo (black dashed line) and total leaf area index (green line)
25 across each ensemble member of the HadCM3C A1B PPE.

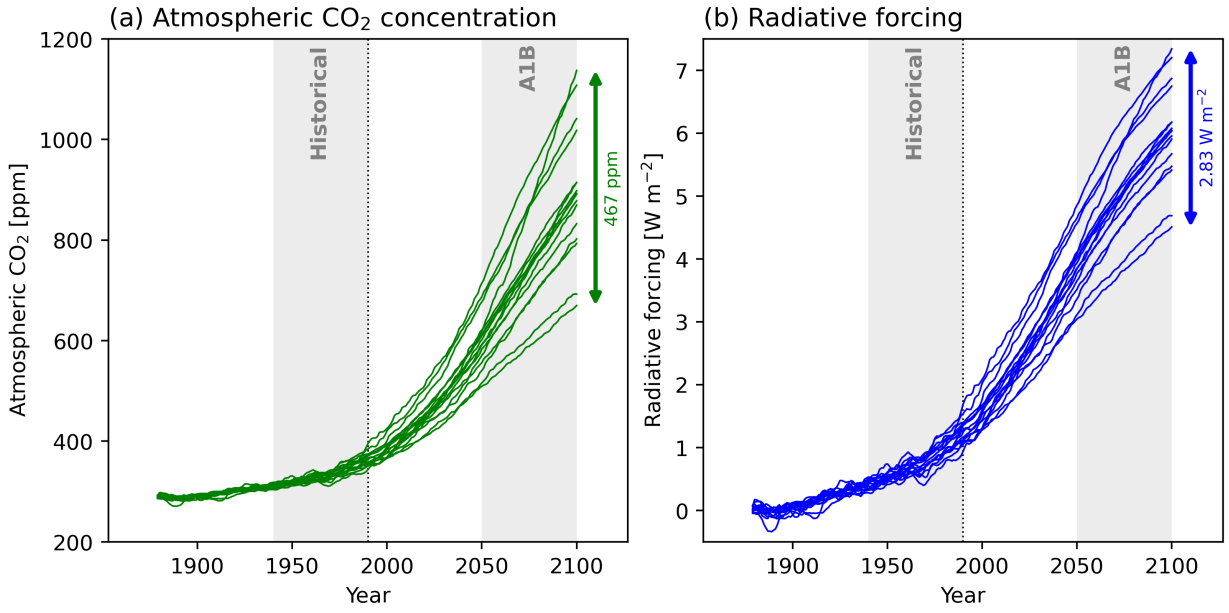

FIG. S4. The time series of (a) global atmospheric CO_2 concentration and (b) the corresponding radiative forcing across the HadCM3C PPE. The radiative forcing was computed as $\Delta RF = 5.35 \ln(C/C_0)$ following Myhre et al. (1998) where C is CO_2 concentration and C_0 is the mean CO_2 concentration over the first 20 years of the control simulation. The highlighted gray regions depict the 50-year averaging periods used in our analysis.

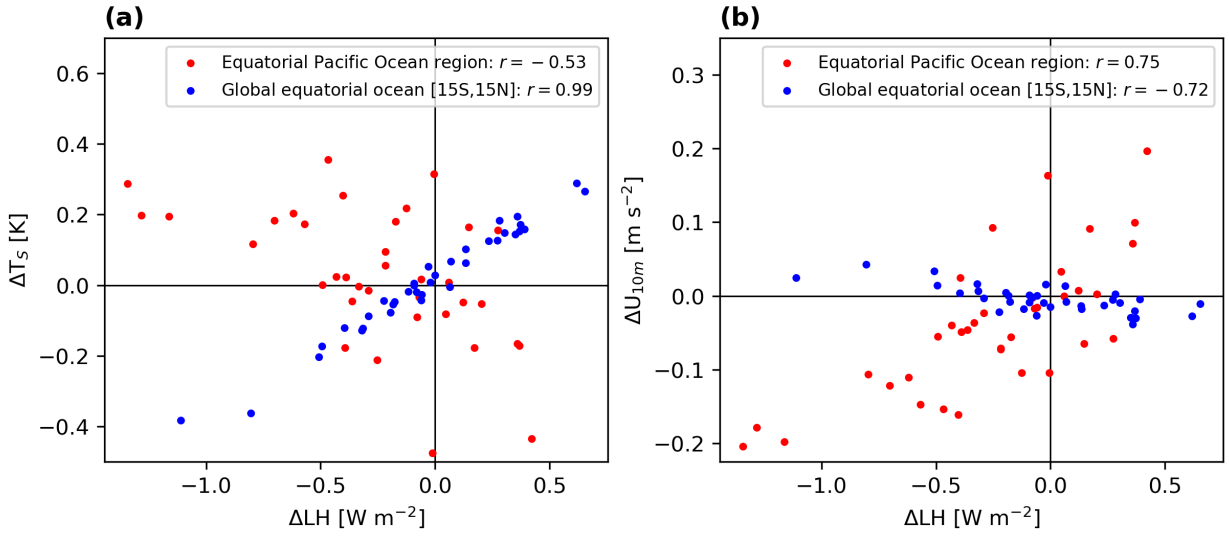

FIG. S5. To understand why evaporation decreases with warming over the equatorial Pacific Ocean in the CESM2 PI PPE, we correlate the change in (a) temperature (T_s) and (b) near-surface wind speed (U_{10m}) with the change in evaporation in energy units (latent heat flux, LH) over the equatorial Pacific Ocean region (red markers) and over the global equatorial ocean (blue markers).

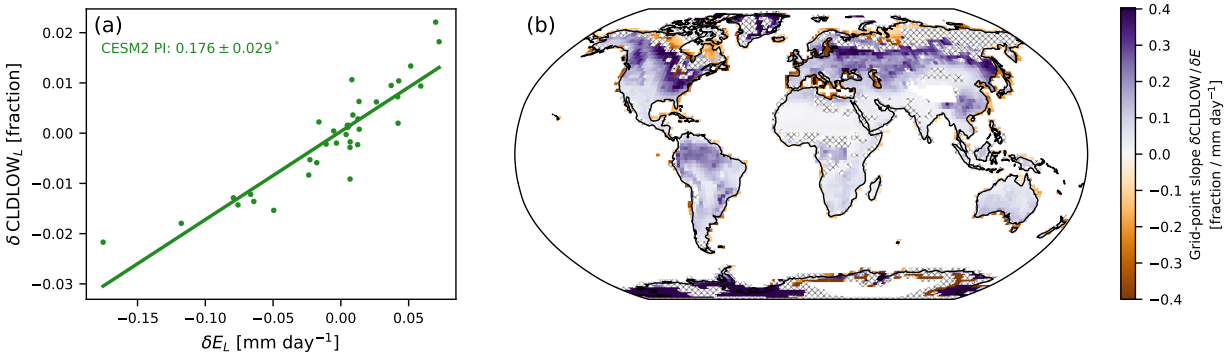

FIG. S6. (a) The change in low cloud fraction (CLDLOW), defined as the cloud fraction below 700 hPa, plotted against the change in ET for each member of the CESM2 PI PPE. (b) A map of the grid-point slope of CLDLOW per unit ET from a least squares regression across the CESM2 PI PPE.

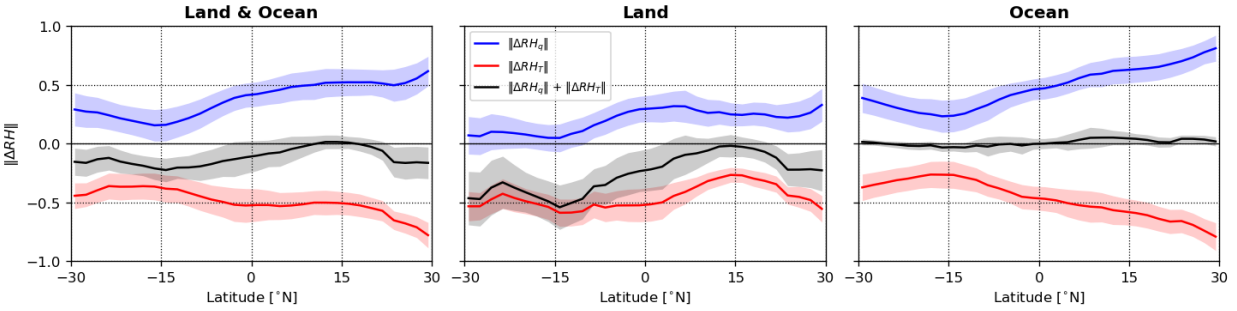

FIG. S7. The zonal and ensemble mean of the temperature-normalized change in near-surface relative humidity. The change in relative humidity was partitioned into specific humidity and temperature contributions following Kim et al. (2020). The specific humidity contribution is defined as $\Delta RH_q = \frac{q'}{q^*} - \frac{q}{q^*}$ and the temperature contribution is defined as $\Delta RH_T = \frac{q}{q^{*'}} - \frac{q}{q^*}$, where q is the specific humidity, q^* is the saturation specific humidity, and the perturbation values are denoted by the prime symbol. To normalize, for each ensemble member we first compute the zonal mean changes in relative humidity and divide by the global mean temperature change. We then aggregate these values into a single array containing all ensemble members and divide by the infinity norm of the array, defined as $\|\mathbf{x}\|_\infty = \max_i |x_i|$. These normalized values are constrained to the range [-1,1] while still retaining their sign and the relative differences between ensemble members. The ensemble mean is then computed and the shading indicates the 95% confidence interval from a one-sample t-test.

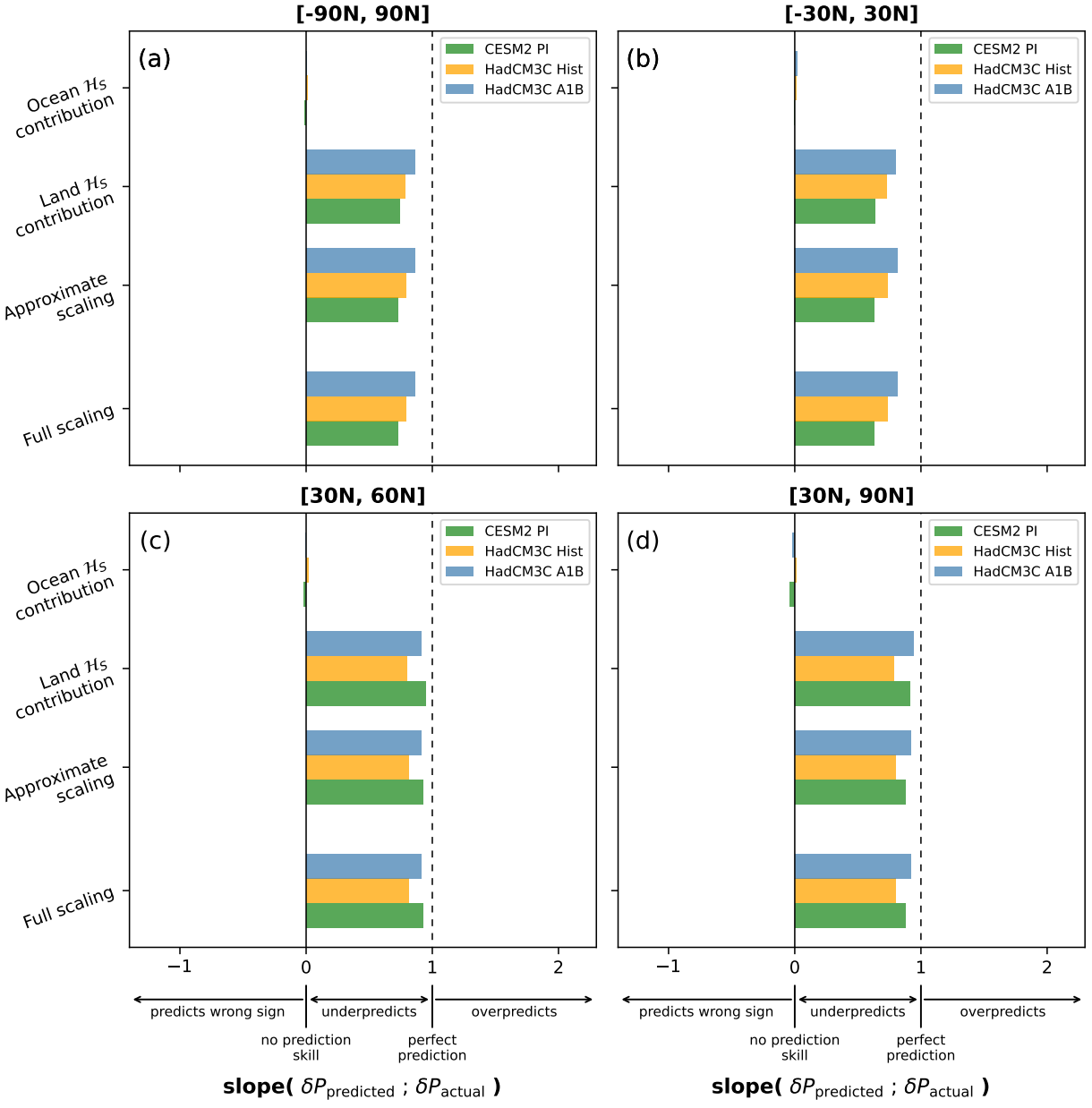

47 FIG. S8. The precipitation change from the compositing scheme plotted as the slope from the ordinary least
48 squares regression of actual and predicted land δP over (a) [–90°N, 90°N], (b) [-30°N, 30°N], (c) [30°N, 60°N],
49 and (d) [30°N, 90°N].

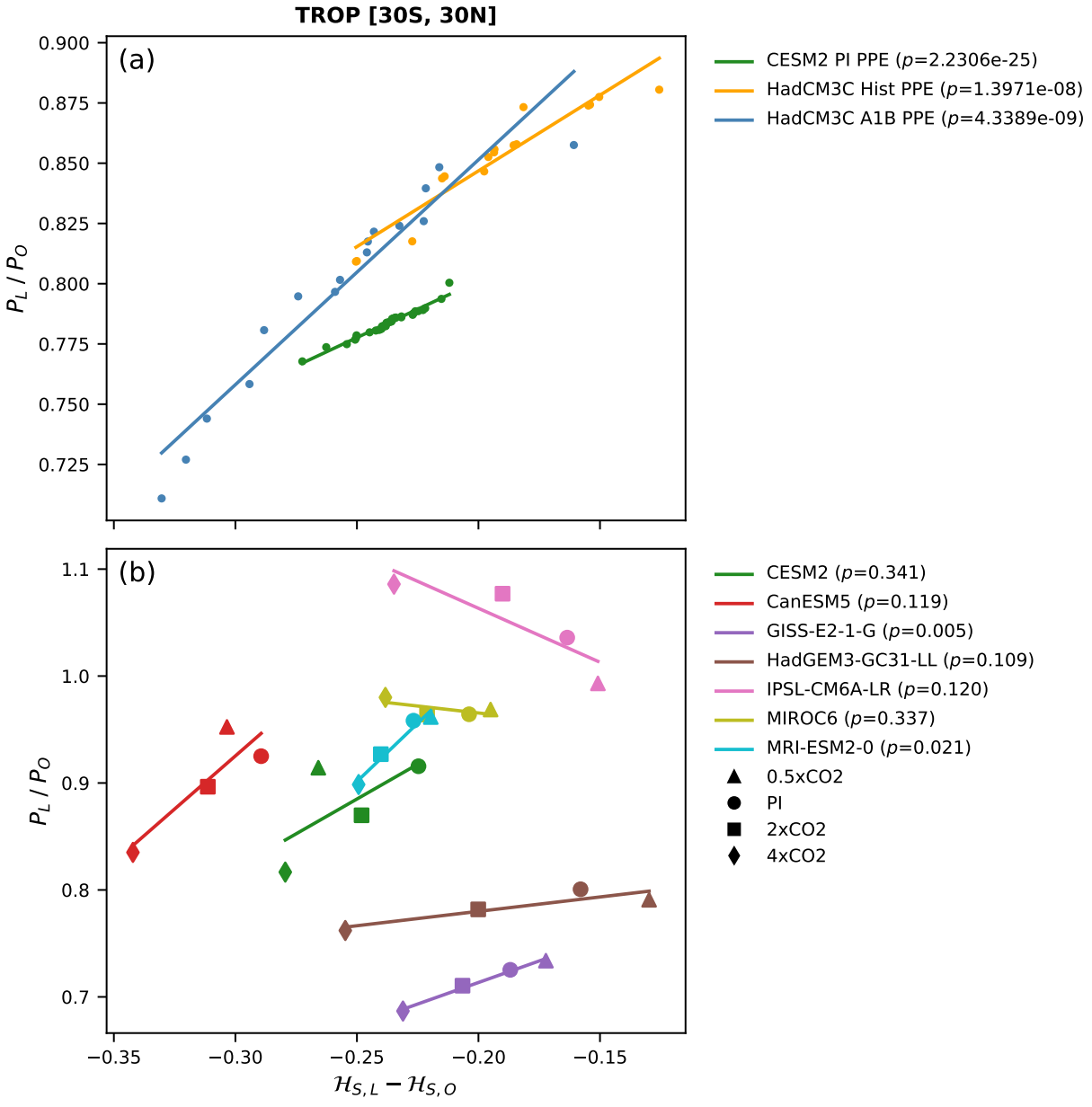

FIG. S9. The regression of $\overline{P}_L/\overline{P}_O = a_1 + a_2(\overline{\mathcal{H}}_{s,L} - \overline{\mathcal{H}}_{s,O})$ for (a) the CESM2 PI, HadCM3 Hist, and HadCM3 A1B PPEs, and for (b) each CMIP6 model in the CO_2 ensemble. The regression coefficients and significance statistics are displayed in Table S5.

TABLE S1. The land parameters perturbed in the CESM2 PI PPE. Each parameter was perturbed to a minimum and maximum value determined by literature review and expert judgement (Kennedy et al. 2025). Percentages indicate a percent perturbation from the default value. Parameters with a "pft" subscript are assigned values for each of the 15 natural vegetation plant functional types (PFTs) in CLM5. Bracketed values represent the minimum and maximum across the PFTs, which were perturbed individually (e.g., `medlynslope`), as a single percent perturbation across all PFTs (e.g., `z0mr`), or all set to a single value (e.g., `nstem`). We note that both the minimum and maximum `medlynslope` values were above the default value for the C3 Arctic grass PFT. Additionally, the minimum and maximum `nstem` values were set to 0.01 and 0.5, respectively, which is below the `nstem` values for the grass PFTs (C3 Arctic grass, C3 non-Arctic grass, and C4 grass). The parameter files are uploaded to our Dryad data repository (Buchovecky et al. 2026).

Parameter Name	Parameter Description	Land Component	Parameter Category	Units	Default Value	Min Value	Max Value
d_max	maximum dry surface layer thickness	soil	soil hydrology	mm	15	10	60
fff	decay factor for fractional saturated area	soil	soil hydrology	m^{-1}	0.5	0.02	5
frac_sat_soil_dsl_init	fraction of soil saturation at which dry surface layer initiates	soil	soil hydrology	unitless	0.8	0.5	1
sand_pf	perturbation factor (via addition) for percent sand	soil	soil hydrology	fraction	1	–20%	+20%
jmaxb0	baseline proportion of nitrogen allocated for electron transport	vegetation	plant photosynthetic capacity	unitless	0.0311	0.01	0.05
jmaxb1	coefficient determining the response of electron transport rate to light availability	vegetation	plant photosynthetic capacity	unitless	0.17	0.05	0.25
$kmax_{pft}$	plant segment maximum conductance	vegetation	plant hydraulics	s^{-1}	[1.3e–9, 4.0e–8]	[2.3e-10, 1.5e–8]	[1.9e–9, 2.3e–7]
lmrha	activation energy for leaf maintenance respiration (used in temperature acclimation of leaf maintenance respiration)	vegetation	plant temperature acclimation	J mol^{-1}	46,390	–50%	+50%
maximum_leaf_wetted_fraction	maximum fraction of leaf that may be wet prior to drip occurring	vegetation	canopy evaporation	fraction	0.05	0.01	0.5
$medlynintercept_{pft}$	intercept of Medlyn stomatal conductance–photosynthesis relationship	vegetation	plant stomatal conductance and water use efficiency	µmol H_2O m^{-2} s^{-1}	100	1	50000
$medlynslope_{pft}$	slope of Medlyn stomatal conductance–photosynthesis relationship	vegetation	plant stomatal conductance and water use efficiency	µmol H_2O (µmol CO_2)$^{-1}$	[1.62, 5.79]	[0.65, 3.89]	[3.93, 9.11]
$nstem_{pft}$	number of stems per meter squared	vegetation	biomass heat storage	number m^{-2}	[0.035, 100]	0.03	0.5
$rhosnir_{pft}$	near-infrared stem reflectance	vegetation	plant optical properties	fraction	[0.36, 0.53]	–20%	+20%
tpu25ratio	triose phosphate utilization at 25C (ratio of tpu25/vcmax25)	vegetation	plant photosynthetic capacity	unitless	0.167	–50%	+200%
$z0mr_{pft}$	ratio of momentum roughness length to canopy top height	boundary layer	boundary layer and roughness length	unitless	[0.055, 0.120]	–40%	+40%
zsno	momentum roughness length for snow	boundary layer	boundary layer and roughness length	m	0.0024	0.00001	0.07
upplim_destruct_metamorph	upper limit for snow densification through destructive metamorphism	boundary layer	snow	kg m^{-3}	175	100	250
zetamaxstable	maximum value zeta ("height" used in Monin-Obukhov theory) can reach under stable conditions	boundary layer	snow	unitless	0.5	0.1	10

TABLE S2. Parameter values for the HadCM3 Hist and A1B PPE (members A–P and control) for six effective parameters (N_{L0}, f_0, minLAI, Q_{10}, θ_{crit}, and T_{opt}) across five plant functional types (broadleaf tree, needleleaf tree, C3 grass, C4 grass, and shrub). Table remade from Booth et al. (2012).

	Control	A	B	C	D	E	F	G	H	I	J	K	L	M	N	O	P
N_{L0}, top leaf nitrogen concentration as a fraction of carbon content [kg N (kg C)$^{-1}$]																	
Broadleaf	0.03	0.018	0.029	0.062	0.073	0.084	0.056	0.067	0.089	0.078	0.095	0.034	0.023	0.100	0.051	0.045	0.040
Needleleaf	0.03	0.024	0.029	0.045	0.055	0.066	0.041	0.050	0.071	0.061	0.077	0.031	0.026	0.082	0.039	0.036	0.034
C3 grass	0.06	0.028	0.045	0.094	0.111	0.127	0.086	0.102	0.135	0.119	0.144	0.053	0.036	0.152	0.078	0.069	0.061
C4 grass	0.03	0.018	0.041	0.108	0.131	0.154	0.097	0.120	0.165	0.142	0.176	0.052	0.029	0.188	0.086	0.075	0.063
Shrub	0.03	0.018	0.028	0.060	0.070	0.080	0.054	0.065	0.086	0.075	0.091	0.034	0.023	0.096	0.049	0.044	0.039
f_0, maximum ratio of leaf internal to external CO_2 concentration [unitless]																	
Broadleaf	0.875	0.930	0.920	0.770	0.95	0.940	0.723	0.747	0.863	0.700	0.900	0.910	0.840	0.817	0.880	0.890	0.793
Needleleaf	0.875	0.930	0.920	0.770	0.95	0.940	0.723	0.747	0.863	0.700	0.900	0.910	0.840	0.817	0.880	0.890	0.793
C3 grass	0.9	0.930	0.920	0.770	0.95	0.940	0.723	0.747	0.863	0.700	0.900	0.910	0.840	0.817	0.880	0.890	0.793
C4 grass	0.8	0.780	0.770	0.680	0.80	0.790	0.660	0.670	0.720	0.650	0.750	0.760	0.710	0.700	0.730	0.740	0.690
Shrub	0.9	0.930	0.920	0.770	0.95	0.940	0.723	0.747	0.863	0.700	0.900	0.910	0.840	0.817	0.880	0.890	0.793
minLAI, minimum leaf area index that a plant functional type (PFT) needs before competing with other PFTs for space [m^2 m^{-2}]																	
Broadleaf	3.0	1.8	1.2	1.6	1.0	3.4	3.2	2.6	3.8	1.4	2.4	3.6	4.0	2.0	2.8	2.2	3.0
Needleleaf	3.0	1.8	1.2	1.6	1.0	3.4	3.2	2.6	3.8	1.4	2.4	3.6	4.0	2.0	2.8	2.2	3.0
Q_{10}, dependence of soil respiration on temperature [unitless]																	
	2.0	2.50	3.30	1.57	1.83	1.63	1.77	2.10	2.70	3.10	1.50	2.90	3.50	1.97	2.30	1.70	1.90
θ_{crit}, critical level of volumetric soil moisture* [unitless]																	
	*	0.141	0.925	0.337	0.206	0.402	0.467	0.533	0.271	0.859	0.794	0.663	0.010	0.729	0.598	0.075	0.990
T_{opt}, optimal temperature for photosynthesis [°C]																	
Broadleaf	32	31.00	33.67	36.33	35.67	27.67	31.67	27.0	29.00	29.67	33.00	32.33	37.0	34.33	28.33	30.33	35.00
Needleleaf	27	26.00	28.67	31.33	30.67	22.67	26.67	22.0	24.00	24.67	28.00	27.33	32.0	29.33	23.33	25.33	30.00
C3 grass	32	31.00	33.67	36.33	35.67	27.67	31.67	27.0	29.00	29.67	33.00	32.33	37.0	34.33	28.33	30.33	35.00
C4 grass	41	40.00	42.67	45.33	44.67	36.67	40.67	36.0	38.00	38.67	42.00	41.33	46.0	43.33	37.33	39.33	44.00
Shrub	32	31.00	33.67	36.33	35.67	27.67	31.67	27.0	29.00	29.67	33.00	32.33	37.0	34.33	28.33	30.33	35.00

* θ_{crit} is defined for the parameter perturbations as a fraction of the difference between the wilting point θ_{wilt} and the saturation point θ_{sat} (i.e., values nearer to unity imply a critical water content nearer saturation). In the control run, there is no single value for this fraction because it depends weakly on soil type. The mean control fraction is approximately 0.37 across soil types.

TABLE S3. CMIP6 models used for the CO_2 ensemble in this study.

Modeling Center	Model Name	Atmosphere Grid	Vertical Levels	Reference
NCAR	CESM2	$1.25° \times 0.9°$	32	Danabasoglu et al. (2020)
CCCma	CanESM5	$2.8° \times 2.8°$	49	Swart et al. (2019)
NASA-GISS	GISS-E2-1-G	$2.5° \times 2°$	40	Kelley et al. (2020)
MOHC	HadGEM3-GC3-LL	$1.875° \times 1.25°$	85	Kuhlbrodt et al. (2018)
IPSL	IPSL-CM6A-LR	$2.5° \times 1.25°$	79	Boucher et al. (2020)
MIROC	MIROC6	$1.4° \times 0.7°$	81	Tatebe et al. (2019)
MRI	MRI-ESM2-0	$1.125° \times 0.56°$	80	Yukimoto et al. (2019)

TABLE S4. Statistics from the least squares regression of $\overline{P}_L/\overline{P}_O \approx a_1 + a_2(\overline{\mathcal{H}}_{s,L} - \overline{\mathcal{H}}_{s,O})$ across each CMIP6 model and each PPE.

Model	a_1	a_2	R^2	p–value
CESM2 CO_2	1.210	1.300	0.434	0.341
CanESM5 CO_2	1.521	1.987	0.777	0.119
GISS-E2-1-G CO_2	0.875	0.806	0.989	0.00531
HadGEM3-GC31-LL CO_2	0.834	0.269	0.794	0.109
IPSL-CM6A-LR CO_2	0.862	–1.009	0.774	0.120
MIROC6 CO_2	0.914	–0.259	0.439	0.337
MRI-ESM2-0 CO_2	1.447	2.183	0.959	0.0207
CESM2 PI PPE	0.895	0.471	0.960	2.23e–25
HadCM3 Hist PPE	0.973	0.629	0.906	1.40e–8
HadCM3 A1B PPE	1.038	0.933	0.921	4.34e–9

References

Booth, B. B. B., and Coauthors, 2012: High sensitivity of future global warming to land carbon cycle processes. *Environmental Research Letters*, **7 (2)**, 024 002, https://doi.org/10.1088/1748-9326/7/2/024002.

Boucher, O., and Coauthors, 2020: Presentation and Evaluation of the IPSL-CM6A-LR Climate Model. *Journal of Advances in Modeling Earth Systems*, **12 (7)**, e2019MS002 010, https://doi.org/10.1029/2019MS002010.

Buchovecky, B. G., F. H. Lambert, C. M. Zarakas, M. M. Laguë, C. D. Koven, I. Y. Fung, D. B. Bonan, and A. L. S. Swann, 2026: Data from: "Reduced Evapotranspiration Decreases Land Precipitation Despite Enhanced Moisture Convergence: Insights from Perturbed Parameter Ensembles of Earth System Models". Dryad, https://doi.org/10.5061/dryad.8kprr4z23.

Danabasoglu, G., and Coauthors, 2020: The Community Earth System Model Version 2 (CESM2). *Journal of Advances in Modeling Earth Systems*, **12 (2)**, e2019MS001 916, https://doi.org/10.1029/2019MS001916.

Kelley, M., and Coauthors, 2020: GISS-E2.1: Configurations and Climatology. *Journal of Advances in Modeling Earth Systems*, **12 (8)**, e2019MS002 025, https://doi.org/10.1029/2019MS002025.

Kennedy, D., and Coauthors, 2025: One-at-a-Time Parameter Perturbation Ensemble of the Community Land Model, Version 5.1. *Journal of Advances in Modeling Earth Systems*, **17 (8)**, e2024MS004 715, https://doi.org/10.1029/2024MS004715.

Kim, J. E., M. M. Laguë, S. Pennypacker, E. Dawson, and A. L. S. Swann, 2020: Evaporative Resistance is of Equal Importance as Surface Albedo in High-Latitude Surface Temperatures Due to Cloud Feedbacks. *Geophysical Research Letters*, **47 (4)**, e2019GL085 663, https://doi.org/10.1029/2019GL085663.

Kuhlbrodt, T., and Coauthors, 2018: The Low-Resolution Version of HadGEM3 GC3.1: Development and Evaluation for Global Climate. *Journal of Advances in Modeling Earth Systems*, **10 (11)**, 2865–2888, https://doi.org/10.1029/2018MS001370.

Myhre, G., E. J. Highwood, K. P. Shine, and F. Stordal, 1998: New estimates of radiative forcing due to well mixed greenhouse gases. *Geophysical Research Letters*, **25 (14)**, 2715–2718, https://doi.org/10.1029/98GL01908.

Swart, N. C., and Coauthors, 2019: The Canadian Earth System Model version 5 (CanESM5.0.3). *Geoscientific Model Development*, **12 (11)**, 4823–4873, https://doi.org/10.5194/gmd-12-4823-2019.

Tatebe, H., and Coauthors, 2019: Description and basic evaluation of simulated mean state, internal variability, and climate sensitivity in MIROC6. *Geoscientific Model Development*, **12 (7)**, 2727–2765, https://doi.org/10.5194/gmd-12-2727-2019.

Yukimoto, S., and Coauthors, 2019: The Meteorological Research Institute Earth System Model Version 2.0, MRI-ESM2.0: Description and Basic Evaluation of the Physical Component. *Journal of the Meteorological Society of Japan. Ser. II*, **97 (5)**, 931–965, https://doi.org/10.2151/jmsj.2019-051.